Available online at www.sciencedirect.com
SCIENCE DIRECT®
Journal of Sound and Vibration 272 (2004) 137–154
JOURNAL OF SOUND AND VIBRATION
www.elsevier.com/locate/jsvi

Free in-plane vibration of an axially moving membrane

Changho Shin[a], Wonsuk Kim[b], Jintai Chung[c,*]

[a] *Department of Precision Mechanical Engineering, Hanyang University, 17 Haengdang-dong, Seongdong-gu, Seoul 133-791, South Korea*

[b] *BK21 Division for Research and Education in Mechanical Engineering, Hanyang University, 17 Haengdang-dong, Seongdong-gu, Seoul 133-791, South Korea*

[c] *Department of Mechanical Engineering, Hanyang University, 1271 Sa-1-dong, Ansan, Kyunggi-do 425-791, South Korea*

Received 10 September 2002; accepted 20 March 2003

Abstract

The free in-plane vibration of an axially moving membrane is studied considering the effects of both the translating speed and aspect ratio of the membrane. Two sets of boundary conditions, which are free and fixed constraints in the lateral direction at boundaries with mass transport, are discussed in this study. From the extended Hamilton principle, the coupled equations of the longitudinal and lateral motions are derived. These equations are then discretized by using the Galerkin method. From the discretized equations, the natural frequencies and mode shapes are obtained for the variations of the translating speed and aspect ratio. The results show that the translating speed, aspect ratio, and boundary conditions have significant effects on the in-plane vibrations of the moving membrane.

1. Introduction

Axially moving material problems have been interesting research subjects for a long time because these problems can be found in many applications such as paper-web handling, magnetic tape recording, belt drives, band-saw blades and so on. These systems are usually modelled as moving membranes or plates to analyze their vibration characteristics. In general, the out-of-plane vibration of such systems has been mainly investigated because their lowest natural frequencies tend to be much lower than the natural frequencies of the in-plane vibration [1].

Although the in-plane vibration has less attention than the out-of-plane vibration, the in-plane vibration may be very important in some cases [1,2]. For example, in a magnetic tape recording

*Corresponding author. Tel.: +82-31-400-5287; fax: +82-31-406-5550.
E-mail address: jchung@hanyang.ac.kr (J. Chung).

0022-460X/03/$ - see front matter
doi:10.1016/S0022-460X(03)00323-7

called a helical scan, a tape is spirally wrapped around a spinning drum, and the heads of the drum contact the tape surface. The mechanism causes the in-plane vibration that results in tension fluctuation and image jitter. Axial motions of flexible materials within cylindrical guides or rollers are also influenced by the in-plane vibration. Kobayashi et al. [3] studied the in-plane vibration of point-supported rectangular plates, and examined the natural frequencies and mode shapes affected by the location of the supports. Bercin [4] assessed the effects and importance of in-plane vibrations by using the dynamic stiffness technique. Bardell et al. [1] presented the in-plane vibrations of isotropic rectangular plates with three different boundary conditions and two aspect ratios. Hyde et al. [2] recently examined the natural frequencies and mode shapes of the in-plane vibration. They carried out parametric studies over a wide range of aspect ratios for three sets of boundary conditions. Liew et al. [5] also analyzed the three-dimensional vibrations of rectangular plates using the Ritz energy approach.

All the previous studies on the in-plane vibration of membranes and plates were not for moving ones but for stationary ones. Thus the translating speed of moving membranes or plates has not been considered yet. However, the translating speed should be included in the dynamic analysis of moving materials, because it is primarily related to the vibration and dynamic characteristics. On the other hand, Chung et al. [6] recently investigated the longitudinal and transverse vibrations of an axially moving string with translating speed. But the results of their study cannot be applicable to axially moving membrane or plate systems with a small length-to-width ratio.

In the present paper, a model of an axially moving rectangular membrane is established for the in-plane vibration analysis. For this purpose, equations of motion are derived by the extended Hamilton principle [7]. Two kinds of boundary conditions are considered at the boundaries with mass transport: fixed and free boundary conditions in the lateral direction. The weak form associated with the equations of motion and boundary conditions is then discretized by the Galerkin method. Finally, to investigate the dynamic characteristics of an axially moving membrane, the natural frequencies and mode shapes are obtained for various aspect ratios and translating speeds.

2. In-plane vibration model and equations of motion

The basic configuration of the in-plane vibration model for an axially moving membrane with length L, width b and thickness h is illustrated in Fig. 1. The membrane is moving with a constant translating speed V in the x direction and the tension per unit length is denoted by T. The xyz

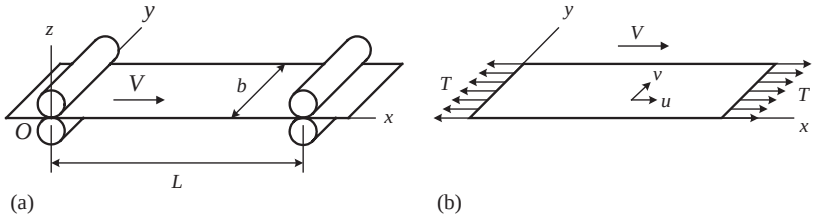

Fig. 1. Schematics of an axially moving membrane: (a) a transport system; and (b) a model of the membrane with the longitudinal and lateral deflections.

co-ordinate system is a space-fixed inertial frame. Note that the longitudinal displacement u and the lateral displacement v are functions of time t as well as the x and y co-ordinates.

When the membrane is in the in-plane motion, the relations between strains and displacements are expressed as

$$\varepsilon_x = \frac{\partial u}{\partial x}, \quad \varepsilon_y = \frac{\partial v}{\partial y}, \quad \varepsilon_{xy} = \frac{1}{2}\left(\frac{\partial u}{\partial y} + \frac{\partial v}{\partial x}\right), \tag{1}$$

where the longitudinal displacement u and the lateral displacement v are displacements in x and y directions, respectively. Since the thickness of the membrane is very small compared to other dimensions, the stresses associated with the z direction can be assumed to be zero, i.e.,

$$\sigma_z = \sigma_{xz} = \sigma_{yz} = 0, \tag{2}$$

and the non-zero stresses are given by

$$\sigma_x = \frac{E}{1-\nu^2}(\varepsilon_x + \nu\varepsilon_y), \quad \sigma_y = \frac{E}{1-\nu^2}(\nu\varepsilon_x + \varepsilon_y), \quad \sigma_{xy} = \frac{E}{1+\nu}\varepsilon_{xy}, \tag{3}$$

where E is the Young's modulus and ν is the Poisson ratio. The strain energy of the membrane can then be obtained from

$$U = \frac{1}{2}h\int_A (\sigma_x\varepsilon_x + \sigma_y\varepsilon_y + 2\sigma_{xy}\varepsilon_{xy})\,\mathrm{d}A, \tag{4}$$

where h is the thickness of the membrane and A is the area.

On the other hand, the position vector of a point on the deformed membrane can be written as

$$\mathbf{r} = (x+u)\mathbf{i} + (y+v)\mathbf{j}, \tag{5}$$

where $\mathbf{i}$ and $\mathbf{j}$ are the unit vectors in the x and y directions, respectively. Then, the velocity vector can be expressed as

$$\mathbf{v} = \left(V + \frac{\partial u}{\partial t} + V\frac{\partial u}{\partial x}\right)\mathbf{i} + \left(\frac{\partial v}{\partial t} + V\frac{\partial v}{\partial x}\right)\mathbf{j}. \tag{6}$$

The kinetic energy of the moving membrane, K, is computed by

$$K = \frac{1}{2}\rho h\int_A \mathbf{v}\cdot\mathbf{v}\,\mathrm{d}A, \tag{7}$$

where ρ is the mass density of the membrane.

The equations of motion and the corresponding boundary conditions can be obtained by using the extended Hamilton principle that is valid for an open system with mass transport. The extended Hamilton principle may be expressed as

$$\int_{t_1}^{t_2} (\delta K - \delta U + \delta W_{nc} - \delta M)\,\mathrm{d}t = 0, \tag{8}$$

where δW_{nc} is the virtual work done by non-conservative forces and δM is the virtual momentum transport across system boundaries. These two terms are given by

$$\delta W_{nc} = \int_0^b T(\delta u|_{x=L} - \delta u|_{x=0})\,\mathrm{d}y, \quad \delta M = \int_\Gamma \rho h(\mathbf{v}\cdot\delta\mathbf{r})(V\mathbf{i}\cdot\mathbf{n})\,\mathrm{d}\Gamma, \tag{9}$$

where Γ is the boundary with mass transport and $\mathbf{n}$ is the outward normal vector at the boundary Γ. By substituting Eqs. (4), (7) and (9) into Eq. (8), the equations of motion for the axially moving membrane are obtained as follows

$$\rho h\left(\frac{\partial^2 u}{\partial t^2}+2V\frac{\partial^2 u}{\partial t\partial x}+V^2\frac{\partial^2 u}{\partial x^2}\right)-\frac{\partial q_x}{\partial x}-\frac{\partial q_{xy}}{\partial y}=0, \tag{10}$$

$$\rho h\left(\frac{\partial^2 v}{\partial t^2}+2V\frac{\partial^2 v}{\partial t\partial x}+V^2\frac{\partial^2 v}{\partial x^2}\right)-\frac{\partial q_y}{\partial y}-\frac{\partial q_{xy}}{\partial x}=0, \tag{11}$$

where

$$q_x=\frac{Eh}{1-\nu^2}\left(\frac{\partial u}{\partial x}+\nu\frac{\partial v}{\partial y}\right),\quad q_y=\frac{Eh}{1-\nu^2}\left(\frac{\partial v}{\partial y}+\nu\frac{\partial u}{\partial x}\right),\quad q_{xy}=\frac{Eh}{2(1+\nu)}\left(\frac{\partial u}{\partial y}+\frac{\partial v}{\partial x}\right). \tag{12}$$

Note that Eqs. (10) and (11) are linear partial differential equations, which are coupled between the longitudinal displacement u and the lateral displacement v. If the translating speed is zero, the equations of motion reduce to

$$\rho\frac{\partial^2 u}{\partial t^2}-\frac{E}{1-\nu^2}\left(\frac{\partial^2 u}{\partial x^2}+\nu\frac{\partial^2 v}{\partial x\partial y}\right)-\frac{E}{2(1+\nu)}\left(\frac{\partial^2 u}{\partial y^2}+\frac{\partial^2 v}{\partial x\partial y}\right)=0, \tag{13}$$

$$\rho\frac{\partial^2 v}{\partial t^2}-\frac{E}{1-\nu^2}\left(\frac{\partial^2 v}{\partial y^2}+\nu\frac{\partial^2 u}{\partial x\partial y}\right)-\frac{E}{2(1+\nu)}\left(\frac{\partial^2 v}{\partial x^2}+\frac{\partial^2 u}{\partial x\partial y}\right)=0, \tag{14}$$

which can be verified by the corresponding equations in Ref. [2]. The associated boundary conditions can be also obtained from Eq. (8). The boundary conditions at the edges of $x=0$ and L are given by

$$q_x=T\quad\text{at } x=0,L, \tag{15}$$

$$q_{xy}\,\delta v=0\quad\text{at } x=0,L. \tag{16}$$

Note that Eqs. (15) and (16) are related to the boundary conditions in the longitudinal and lateral directions, respectively. The relation in Eq. (15) means that the membrane is subject to a constant tension T along the mass-transport boundaries at $x=0$ and L when the translating speed is not varying. The boundary conditions of moving materials have been studied by many researchers using various models for moving strings or sliding beams. For example, Chung et al. [6] treated a moving string with translating acceleration, and obtained time responses of the in-plane displacement. They also calculated the natural frequencies of the system when the string was moving at constant speed. In that case, the boundary conditions at supports were the same as those in Eq. (15). In fact, the realistic treatment of boundary conditions for moving material systems is a very difficult subject, and still problematic. One of the main goals and contributions of this study is to investigate the effects of the lateral dimension of moving membranes on the natural frequencies. Therefore, a great deal of efforts have been focused on the boundary conditions of Eq. (16), which are the lateral boundary conditions at $x=0$, L. Related to the longitudinal boundary conditions at $x=0$, L, the boundary conditions presented by Chung et al. [6] are simply adopted in this paper, as shown in Eq. (15). The boundary conditions in Eq. (16) can be categorized into two cases. The boundary conditions of the first case (Case I) correspond to

$q_{xy} = 0$ at $x = 0$ and L. In this case, no friction and external force exist in the lateral direction. So the membrane can freely move in the y direction. The other case (Case II) is when the lateral displacement is zero, i.e., $v = 0$ at $x = 0$ and L. Case II may correspond to a case with maximum friction, which prevents the slipping of the membrane in the y direction, between the rollers and the membrane. Even though it seems that both the cases are not practical, they will be treated in this study because the actual situation of transport devices may lie between the extremes, namely, Cases I and II. On the other hand, the boundary conditions at the edges of $y = 0$ and b are given by

$$q_y = q_{xy} = 0 \quad \text{at } y = 0,\ b. \tag{17}$$

It can be noted from Eq. (17) that the boundaries are free at $y = 0$ and b.

3. Discretization of the equations of motion

Since the exact solutions of the governing Eqs. (10) and (11) are not feasible, to obtain approximate solutions in a finite-dimensional function space, the discretization is carried out based on the Galerkin method. In this problem, it is very difficult to select the trial functions as the comparison functions that satisfy both the geometric and natural boundary conditions. Thus, the Galerkin method is necessarily applied to the weak form, which can be derived from the strong forms given by the partial differential equations and the corresponding boundary conditions. The weak form is obtained by multiplying Eqs. (10) and (11) by the weighting functions $\bar{u}$ and $\bar{v}$, respectively, summing the equations, and then integrating the resultant equation by parts over the length L and width b as shown in the equation below

$$\int_0^b \int_0^L \left[\rho h\bar{u}\left(\frac{\partial^2 u}{\partial t^2} + 2V\frac{\partial^2 u}{\partial t\partial x} + V^2\frac{\partial^2 u}{\partial x^2}\right) + \frac{\partial \bar{u}}{\partial x}q_x + \frac{\partial \bar{u}}{\partial y}q_{xy}\right] \mathrm{d}x\,\mathrm{d}y$$
$$+ \int_0^b \int_0^L \left[\rho h\bar{v}\left(\frac{\partial^2 v}{\partial t^2} + 2V\frac{\partial^2 v}{\partial t\partial x} + V^2\frac{\partial^2 v}{\partial x^2}\right) + \frac{\partial \bar{v}}{\partial y}q_y + \frac{\partial \bar{v}}{\partial x}q_{xy}\right] \mathrm{d}x\,\mathrm{d}y = \int_0^b T(\bar{u}|_{x=L} - \bar{u}|_{x=0})\,\mathrm{d}y. \tag{18}$$

Since the natural boundary conditions are already considered in the above procedure, the trial functions need to satisfy only the geometric boundary conditions. In other words, the admissible functions can be selected as the trial functions. The longitudinal and lateral displacements may be approximated as

$$u = \sum_{i=0}^{N}\sum_{j=0}^{N} T_{ij}^u(t)Z_{ij}^u(x,y), \quad v = \sum_{i=0}^{N}\sum_{j=0}^{N} T_{ij}^v(t)Z_{ij}^v(x,y), \tag{19}$$

In Eq. (19), N is the total number of the basis functions, $T_{ij}^u(t)$ and $T_{ij}^v(t)$ are unknown functions of time to be determined, and $Z_{ij}^u(x,y)$ and $Z_{ij}^v(x,y)$ may be given by

$$Z_{ij}^u(x,y) = X_i(x)\,Y_j(y), \tag{20}$$

$$Z_{ij}^v(x,y) = \begin{cases} X_i(x)\,Y_j(y) & \text{for Case I,} \\ \sin\dfrac{(i+1)\pi x}{L}\,Y_j(y) & \text{for Case II,} \end{cases} \tag{21}$$

where X_i and Y_j are the Legendre polynomials defined by

$$X_i(x) = \sum_{r=0}^{R_1} (-1)^r \frac{(2i-2r)!}{2^i r!(i-r)!(i-2r)!} \left(\frac{2x}{L} - 1\right)^{i-2r}, \quad i = 0, 1, \ldots, N, \tag{22}$$

$$Y_j(y) = \sum_{r=0}^{R_2} (-1)^r \frac{(2j-2r)!}{2^j r!(j-r)!(j-2r)!} \left(\frac{2y}{b} - 1\right)^{j-2r}, \quad j = 0, 1, \ldots, N, \tag{23}$$

in which

$$R_1 = \begin{cases} i/2 & \text{if } i \text{ is even,} \\ (i-1)/2 & \text{if } i \text{ is odd,} \end{cases} \quad R_2 = \begin{cases} j/2 & \text{if } j \text{ is even,} \\ (j-1)/2 & \text{if } j \text{ is odd.} \end{cases} \tag{24}$$

For Case II, sinusoidal functions are taken instead of X_i to satisfy the geometric boundary conditions given by $v = 0$ at $x = 0$ and L. Similarly, the weighting functions corresponding to the trial functions u and v can be expressed as

$$\bar{u} = \sum_{m=0}^{N} \sum_{n=0}^{N} \bar{T}^u_{mn}(t) Z^u_{mn}(x, y), \quad \bar{v} = \sum_{m=0}^{N} \sum_{n=0}^{N} \bar{T}^v_{mn}(t) Z^v_{mn}(x, y), \tag{25}$$

where $\bar{T}^u_{mn}$ and $\bar{T}^v_{mn}$ are arbitrary functions of time.

Substituting Eqs. (19) and (25) into Eq. (18) and then collecting all the terms in terms of $\bar{T}^u_{mn}$ and $\bar{T}^v_{mn}$, the arbitrariness of $\bar{T}^u_{mn}$ and $\bar{T}^v_{mn}$ provides the discretized equations

$$\sum_{i=0}^{N} \sum_{j=0}^{N} (m^u_{mnij} \ddot{T}^u_{ij} + 2Vg^u_{mnij} \dot{T}^u_{ij} + k^{uu}_{mnij} T^u_{ij} + k^{uv}_{mnij} T^v_{ij}) = f_{mn} \quad \text{for } m, n = 0, 1, \ldots, N, \tag{26}$$

$$\sum_{i=0}^{N} \sum_{j=0}^{N} (m^v_{mnij} \ddot{T}^v_{ij} + 2Vg^v_{mnij} \dot{T}^v_{ij} + k^{vv}_{mnij} T^v_{ij} + k^{vu}_{mnij} T^u_{ij}) = 0 \quad \text{for } m, n = 0, 1, \ldots, N, \tag{27}$$

where the superposed dot indicates differentiation with respect to time t. In Eqs. (26) and (27), the coefficients m^u_{mnij}, g^u_{mnij}, k^{uu}_{mnij} and f_{mn} are defined by

$$m^u_{mnij} = \rho h X^{00}_{mi} Y^{00}_{nj}, \quad g^u_{mnij} = \tfrac{1}{2} \rho h [X^{01}_{mi} - X^{10}_{mi} + 1 - (-1)^{m+i}] Y^{00}_{nj},$$

$$k^{uu}_{mnij} = (D - \rho h V^2) X^{11}_{mi} Y^{00}_{nj} + D_0 X^{00}_{mi} Y^{11}_{nj} + \rho h V^2 [X'_i(L) - (-1)^m X'_i(0)] Y^{00}_{nj},$$

$$f_{mn} = [1 - (-1)^m] T \int_0^b Y_n \, \mathrm{d}y, \tag{28}$$

where the prime denotes differentiation with respect to x; D and D_0 are

$$D = \frac{Eh}{1 - \nu^2}, \quad D_0 = \frac{Eh}{2(1 + \nu)}, \tag{29}$$

and X^{00}_{mi}, X^{01}_{mi}, X^{10}_{mi}, X^{11}_{mi}, Y^{00}_{nj} and Y^{11}_{nj} are given by

$$X^{00}_{mi} = \int_0^L X_m X_i \, \mathrm{d}x, \quad X^{01}_{mi} = \int_0^L X_m \frac{\mathrm{d}X_i}{\mathrm{d}x} \mathrm{d}x, \quad X^{10}_{mi} = \int_0^L \frac{\mathrm{d}X_m}{\mathrm{d}x} X_i \, \mathrm{d}x, \quad X^{11}_{mi} = \int_0^L \frac{\mathrm{d}X_m}{\mathrm{d}x} \frac{\mathrm{d}X_i}{\mathrm{d}x} \mathrm{d}x,$$

$$Y_{nj}^{00} = \int_0^b Y_n Y_j \, \mathrm{d}y, \quad Y_{nj}^{11} = \int_0^b \frac{\mathrm{d}Y_n}{\mathrm{d}y}\frac{\mathrm{d}Y_j}{\mathrm{d}y}\,\mathrm{d}y. \tag{30}$$

On the other hand, the coefficients m_{mnij}^{v}, g_{mnij}^{v}, k_{mnij}^{uv}, k_{mnij}^{vu} and k_{mnij}^{vv} are defined differently for Cases I and II. For Case I, these coefficients are defined by

$$m_{mnij}^{v} = \rho h X_{mi}^{00} Y_{nj}^{00}, \quad g_{mnij}^{v} = 0.5\rho h[X_{mi}^{01} - X_{mi}^{10} + 1 - (-1)^{m+i}]Y_{nj}^{00},$$

$$k_{mnij}^{uv} = vDX_{mi}^{10} Y_{nj}^{01} + D_0 X_{mi}^{01} Y_{nj}^{10}, \quad k_{mnij}^{vu} = vDX_{mi}^{01} Y_{nj}^{10} + D_0 X_{mi}^{10} Y_{nj}^{01},$$

$$k_{mnij}^{vv} = (D_0 - \rho h V^2)X_{mi}^{11} Y_{nj}^{00} + DX_{mi}^{00} Y_{nj}^{11} + \rho h V^2[X_i'(L) - (-1)^m X_i'(0)]Y_{nj}^{00}, \tag{31}$$

while, for Case II, they are defined by

$$m_{mnij}^{v} = \rho h C_{mi}^{00} Y_{nj}^{00}, \quad g_{mnij}^{v} = 0.5\rho h[C_{mi}^{01} - C_{mi}^{10}]Y_{nj}^{00}, \quad k_{mnij}^{uv} = vD\bar{C}_{mi}^{10} Y_{nj}^{01} + D_0 \bar{C}_{mi}^{01} Y_{nj}^{10},$$

$$k_{mnij}^{vu} = vD\bar{C}_{mi}^{10} Y_{nj}^{10} + D_0 \bar{C}_{mi}^{01} Y_{nj}^{01}, \quad k_{mnij}^{vv} = (D_0 - \rho h V^2)C_{mi}^{11} Y_{nj}^{00} + DC_{mi}^{00} Y_{nj}^{11}. \tag{32}$$

In Eqs. (31) and (32), the coefficients Y_{nj}^{01}, Y_{nj}^{10}, C_{mi}^{00}, C_{mi}^{01}, C_{mi}^{10}, C_{mi}^{11}, $\bar{C}_{mi}^{01}$ and $\bar{C}_{mi}^{10}$ are given by

$$Y_{nj}^{01} = \int_0^b Y_n \frac{\mathrm{d}Y_j}{\mathrm{d}y}\,\mathrm{d}y, \quad Y_{nj}^{10} = \int_0^b \frac{\mathrm{d}Y_n}{\mathrm{d}y} Y_j \,\mathrm{d}y, \quad C_{mi}^{00} = \int_0^L \sin\frac{(m+1)\pi x}{L}\sin\frac{(i+1)\pi x}{L}\,\mathrm{d}x,$$

$$C_{mi}^{01} = \frac{(i+1)\pi}{L}\int_0^L \sin\frac{(m+1)\pi x}{L}\cos\frac{(i+1)\pi x}{L}\,\mathrm{d}x, \quad C_{mi}^{10} = \frac{(m+1)\pi}{L}\int_0^L \cos\frac{(m+1)\pi x}{L}\sin\frac{(i+1)\pi x}{L}\,\mathrm{d}x,$$

$$C_{mi}^{11} = \frac{(m+1)(i+1)\pi^2}{L^2}\int_0^L \cos\frac{(m+1)\pi x}{L}\cos\frac{(i+1)\pi x}{L}\,\mathrm{d}x, \quad \bar{C}_{mi}^{01} = \frac{(i+1)\pi}{L}\int_0^L X_m \cos\frac{(i+1)\pi x}{L}\,\mathrm{d}x,$$

$$\bar{C}_{mi}^{10} = \int_0^L \frac{\mathrm{d}X_m}{\mathrm{d}x}\sin\frac{(i+1)\pi x}{L}\,\mathrm{d}x. \tag{33}$$

Eqs. (26) and (27) can be rewritten in the vector-matrix form

$$\mathbf{M}\ddot{\mathbf{S}} + 2V\mathbf{G}\dot{\mathbf{S}} + \mathbf{K}\mathbf{S} = \mathbf{F}, \tag{34}$$

where $\mathbf{M}$ is the mass matrix, $\mathbf{G}$ is the matrix related to the gyroscopic force, $\mathbf{K}$ is the stiffness matrix, $\mathbf{F}$ is the applied load vector, and $\mathbf{S}$ is defined by

$$S = \{T_{00}^{u}, T_{10}^{u}, \ldots, T_{ij}^{u}, \ldots, T_{NN}^{u}, T_{00}^{v}, T_{10}^{v}, \ldots, T_{ij}^{v}, \ldots, T_{NN}^{v}\}^{\mathrm{T}}. \tag{35}$$

Eq. (34) represents the discretized equation of motion for a steady state of the membrane without an applied force.

4. Dynamic analysis

In order to compute the natural frequencies and modal vectors of the moving membrane, it is convenient to transform the homogeneous version of Eq. (34) into

$$\mathbf{A}\dot{\mathbf{T}}(t) + \mathbf{B}\mathbf{T}(t) = \mathbf{0}, \tag{36}$$

where

$$\mathbf{A} = \begin{bmatrix} \mathbf{M} & \mathbf{0} \\ \mathbf{0} & \mathbf{I} \end{bmatrix}, \quad \mathbf{B} = \begin{bmatrix} 2V\mathbf{G} & \mathbf{K} \\ -\mathbf{I} & \mathbf{0} \end{bmatrix}, \quad \mathbf{T}(t) = \begin{Bmatrix} \dot{\mathbf{S}} \\ \mathbf{S} \end{Bmatrix}, \tag{37}$$

in which $\mathbf{I}$ is the identity matrix and $\mathbf{T}(t)$ is the state vector. To obtain the natural frequencies and mode shapes, the solution of Eq. (36) can be assumed as

$$\mathbf{T}(t) = \mathbf{T}_0 e^{\lambda_n t}, \tag{38}$$

where λ_n is the eigenvalue and $\mathbf{T}_0$ is the eigenvector. Substituting Eq. (38) into Eq. (36), the natural frequencies and the modal vectors for the in-plane vibration of a membrane can be obtained from

$$(\mathbf{B} + \lambda_n \mathbf{A})\mathbf{T}_0 = 0. \tag{39}$$

Some numerical results will now be presented for two sets of boundary conditions, Cases I and II. The dimensions of membranes are given as $L = 420\,\text{mm}$ and $h = 25\,\mu\text{m}$, and the material properties of a magnetic tape ($\rho = 1400\,\text{kg/m}^3$, $E = 3.8\,\text{GPa}$ and $v = 0.3$) obtained in Ref. [8] are used in simulations. For convenience of comparison, the dimensionless natural frequency $\bar{\omega}$ and the dimensionless velocity $\bar{V}$ are introduced as follows:

$$\bar{\omega} = \omega / \left[\frac{E}{\rho L^2(1-v^2)}\right]^{1/2}, \quad \bar{V} = V / \left[\frac{E}{\rho(1-v^2)}\right]^{1/2}, \tag{40}$$

where ω is the calculated natural frequency of a membrane.

4.1. Case I: free lateral boundaries at both ends

For the boundary conditions of Case I, i.e., for $q_{xy} = 0$ at $x = 0$ and L, the natural frequencies and corresponding mode shapes are obtained. First of all, the convergence of the natural frequencies is evaluated to verify the discretized equations. Shown in Tables 1 and 2 are the lowest six in-plane natural frequencies of stationary and moving membranes with the aspect ratio of $L/b = 3$, when the boundary conditions are for Case I. It is seen in Tables 1 and 2 that the natural

Table 1
Convergence characteristics of the dimensionless natural frequencies for the stationary membrane with $L/b = 3$ when the boundary conditions are for Case I

N	First	Second	Third	Fourth	Fifth	Sixth
1	3.2863	6.4807	7.0569	10.4499	10.5925	N/A
2	1.8598	3.2863	6.4807	7.0518	8.1333	9.5583
3	1.7270	2.9840	3.9913	6.6191	6.9872	7.2858
4	1.5788	2.9840	3.6860	5.8524	5.8535	6.4163
5	1.5723	2.9831	3.2583	5.6172	5.8501	5.9413
6	1.5707	2.9831	3.2339	5.0307	5.8299	5.8867
7	1.5707	2.9831	3.2225	4.9862	5.7705	5.8298
8	1.5707	2.9831	3.2223	4.9498	5.7611	5.8297

Table 2
Convergence characteristics of the dimensionless natural frequencies for the moving membrane with $\bar{V} = 0.1$ and $L/b = 3$ when the boundary conditions are for Case I

N	First	Second	Third	Fourth	Fifth	Sixth
1	3.2863	6.4807	7.0569	10.4499	10.5925	N/A
2	1.7395	3.2863	6.4807	7.0158	8.1230	9.5273
3	1.5786	2.9517	3.9889	6.6274	7.0197	7.2455
4	1.4144	2.9490	3.7166	5.7871	5.8125	6.4042
5	1.4014	2.9491	3.1872	5.5308	5.7602	5.9563
6	1.3990	2.9491	3.1250	4.9096	5.7356	5.9153
7	1.3990	2.9491	3.1101	4.8005	5.7350	5.8374
8	1.3990	2.9491	3.1083	4.7383	5.7348	5.8293

Table 3
Comparison of the dimensionless natural frequencies for the stationary membrane with boundary conditions of Case I when $L/b = 1$ or 2

$L/b = 1$		$L/b = 2$	
Present ($N = 8$)	Ref. [1]	Present ($N = 8$)	Ref. [1]
2.321	2.321	1.954	1.954
2.472	2.472	2.961	2.961
2.472	2.472	3.267	3.267
2.628	2.628	4.727	4.726
2.987	2.987	4.784	4.784
3.452	3.452	5.205	5.205

frequencies are converged as the number of basis functions N increases. Note that eight basis functions are sufficient for the convergence.

It is now valuable to check whether or not the in-plane natural frequencies obtained from the model of this study are consistent with results in the literature. However, it is impossible to find the results for the in-plane vibration of moving membranes because all the previous studies reported the natural frequencies for not moving but stationary membranes or plates to the authors' knowledge. Thus, in Table 3, the lowest six natural frequencies of *stationary* membranes with the boundary conditions of Case I are compared with the results of Bardell et al. [1]. It is shown that the natural frequencies agree well with each other.

The effects of the translating speed and aspect ratio on the natural frequencies will now be investigated. First, as shown in Fig. 2, the lowest six dimensionless natural frequencies $\bar{\omega}$ are influenced by the dimensionless translating speed $\bar{V}$ when the aspect ratio is $L/b = 3$. The corresponding mode shapes are depicted in Fig. 3 for case of $\bar{V} = 0.01$. Note that, when a membrane is moving, each modal co-ordinate has a different phase angle in general because eigenvectors are complex due to the matrix $\mathbf{G}$ in Eq. (34). Therefore, the modal co-ordinates do

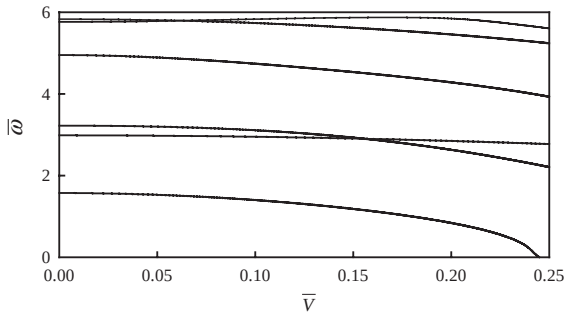

Fig. 2. Dimensionless natural frequencies $\bar{\omega}$ versus the dimensionless translating speed $\bar{V}$ for the membrane of Case I when $L/b = 3$.

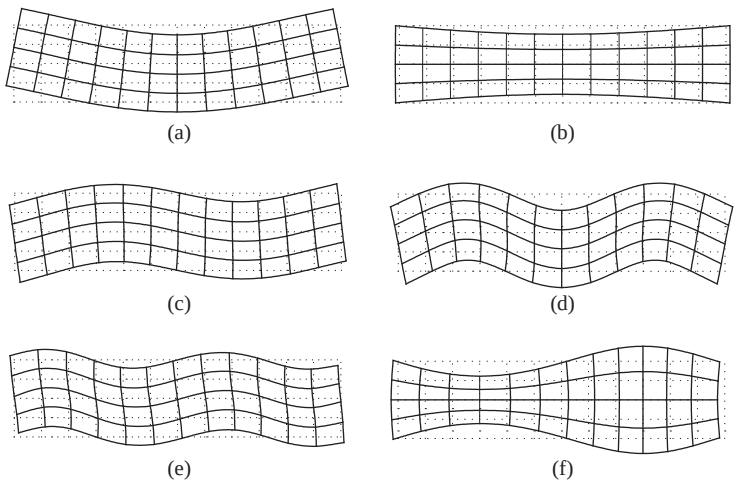

Fig. 3. Mode shapes of the membrane (Case I) when $L/b = 3$ and $\bar{V} = 0.01$: (a) the first mode; (b) the second mode; (c) the third mode; (d) the fourth mode; (e) the fifth mode; and (f) the sixth mode.

not reach their maximum values at the same time, and consequently the mode shapes change with time. However, since the imaginary values are much smaller than the real values of the eigenvectors for the moving membranes of this study, the variation of mode shapes in time due to phase angles is negligible. Thus, the mode shapes obtained from only the real parts of the eigenvectors are plotted at a given time. It is shown in Fig. 3 that the modes of the moving membrane consist of flexural and longitudinal modes. The second and sixth modes can be treated as longitudinal modes, and the others may be considered as flexural modes. As shown in Fig. 2, the natural frequencies are generally decreased as the translating speed increases. This trend can also be found in the vibration of a string [6]. Furthermore, it is observed that the first natural frequency becomes zero at a specific translating speed, $\bar{V} = 0.245$. This speed is a critical speed in a sense of the dynamic instability of the moving membrane. An interesting point to be mentioned here is that the veering phenomena between the frequency loci are observed in Fig. 2. The veering regions are magnified in Fig. 4. It is known that veering phenomena may occur due to the

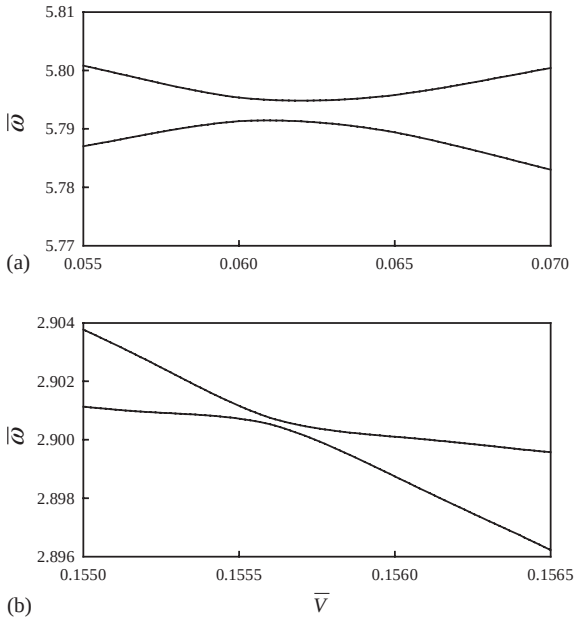

Fig. 4. Veering phenomena of the frequency loci (Case I): (a) the fifth and sixth modes; (b) the second and third modes.

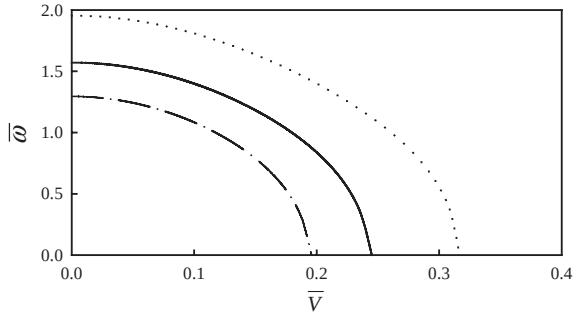

Fig. 5. Comparison of the lowest dimensionless natural frequencies of the moving membrane for Case I when the aspect ratios are $L/b = 2$ (· · ·), 3 (—) and 4 (- · - · - · - ·).

coupling between different modes [9]. The veering phenomenon shown in Fig. 4(a) occurs between the fifth (flexural mode) and sixth modes (longitudinal mode), while the phenomenon shown in Fig. 4(b) occurs between the second (longitudinal mode) and third modes (flexural mode).

Next, consider the effects of the aspect ratio on the natural frequencies. The lowest dimensionless natural frequencies of the moving membranes with the aspect ratios of $L/b =$ 2, 3 and 4 are shown in Fig. 5. It is seen that the magnitudes of the natural frequencies and critical speed decrease as the aspect ratio L/b increases. Fig. 6 shows the lowest four dimensionless natural frequencies as functions of the aspect ratio, where the solid and dotted lines denote $\bar{V} = 0.1$ and 0, respectively. For a stationary membrane, i.e., $\bar{V} = 0$, a similar plot and some useful

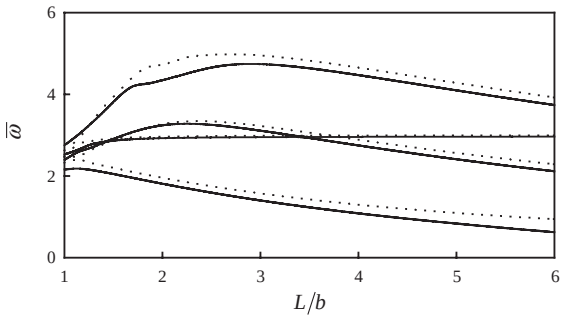

Fig. 6. Dimensionless natural frequencies $\bar{\omega}$ versus the aspect ratio L/b for Case I when $\bar{V} = 0.1$ (—) or $\bar{V} = 0$ ($\cdot\ \cdot\ \cdot$).

Table 4
Convergence characteristics of the dimensionless natural frequencies for the stationary membrane with boundary conditions of Case II when $L/b = 3$

N	First	Second	Third	Fourth	Fifth	Sixth
1	0.9092	3.3254	3.7172	6.1482	7.2407	10.6017
2	0.8670	2.8683	3.3074	5.5199	6.1482	7.2157
3	0.7811	2.7322	2.9840	4.8690	5.5773	6.4655
4	0.7810	2.4057	2.9840	4.8141	5.5773	5.8507
5	0.7808	2.4056	2.9831	4.2523	5.5758	5.8507
6	0.7808	2.3998	2.9831	4.2522	5.5758	5.8300
7	0.7808	2.3997	2.9831	4.2229	5.5758	5.8300
8	0.7808	2.3997	2.9831	4.2197	5.5758	5.8299

comments can be found in Ref. [2]. It is seen that the trends of the frequency loci of the moving membranes (solid lines) are very similar to those of the stationary membranes (dotted lines). However, the frequencies of the moving membranes happen to be lower than those of the stationary ones.

4.2. Case II: fixed lateral boundaries at both ends

For the boundary conditions of Case II, the natural frequencies and corresponding mode shapes are also obtained. First, convergence tests are performed as shown in Tables 4 and 5 for $\bar{V} = 0$ and 0.1, respectively, when the aspect ratio $L/b = 3$. It is noticed that the natural frequencies of the stationary or moving membrane with the boundary conditions of Case II converge with N. Based on the results, $N = 8$ is chosen in further computations.

The next step is to find comparable results in the literature for the purpose of verification. However, it is impossible to find the corresponding results because of two reasons. The first reason is that, as mentioned before, all the previous studies treated only stationary membranes or plates. The other reason is related to boundary conditions. In most of the literature, the boundary conditions for both u and v are simultaneously fixed–fixed, i.e., $u = v = 0$ or free–free, i.e., $u \neq 0$ and $v \neq 0$ along each side of a rectangular membrane. In Case II of this study, the boundary

Table 5
Convergence characteristics of the dimensionless natural frequencies for the moving membrane with boundaries of Case II when $L/b = 3$ and $\bar{V} = 0.1$

N	First	Second	Third	Fourth	Fifth	Sixth
1	0.8472	3.3252	3.7017	6.1482	7.2417	10.4723
2	0.7963	2.7938	3.3068	5.5413	6.1482	7.2159
3	0.6980	2.6562	2.9526	4.7400	5.5773	6.4273
4	0.6939	2.3227	2.9494	4.7054	5.5773	5.8043
5	0.6938	2.2992	2.9493	4.1629	5.5758	5.7715
6	0.6938	2.2893	2.9493	4.1127	5.5758	5.7431
7	0.6937	2.2886	2.9493	4.0689	5.5758	5.7422
8	0.6937	2.2882	2.9493	4.0619	5.5758	5.7419

Table 6
Comparison of the dimensionless natural frequencies for the stationary membrane with boundaries of Case II when $L/b = 3$

$\bar{\omega}$	Present ($N = 8$)	ANSYS	Difference (%)
1	0.7808	0.7814	0.08
2	2.3997	2.4046	0.20
3	2.9831	2.9837	0.02
4	4.2197	4.2377	0.42
5	5.5758	5.5847	0.16
6	5.8299	5.8348	0.08

conditions for u and v at $y = 0$ and b are free–free. However, the boundary conditions at $x = 0$ and L can be represented by $u \neq 0$ (because of mass transport) and $v = 0$ (because of maximum friction). This kind of *mixed* boundary conditions has not been treated in the pervious studies. Therefore, the finite element commercial code, ANSYS, is used in this study to verify the natural frequencies of a *stationary* membrane. Table 6 shows the lowest six dimensionless natural frequencies obtained from the developed model and ANSYS for the stationary membrane of $L/b = 3$. It is seen that both results are in good agreement.

The effects of the dimensionless translating speed $\bar{V}$ on the dimensionless natural frequencies $\bar{\omega}$ are analyzed for $L/b = 3$ as shown in Fig. 7, and the corresponding mode shapes when $\bar{V} = 0.01$ are presented in Fig. 8. The lowest six modes in Fig. 8 consist of the flexural, longitudinal and shear modes. The first, second and fourth modes are the flexural modes, and the third and sixth modes may be considered as longitudinal modes. The fifth mode looks like the shear mode in the longitudinal direction. It seems that the shear mode has no deformation in the lateral direction. In Fig. 7, the natural frequencies of the flexural modes decrease as the translating speed increases. The natural frequencies of the longitudinal modes are also decreased as $\bar{V}$ increases, but the decreasing rates are much lower than those of the flexural modes. Note that this trend is similar to that of Case I. However, it is observed that the shear mode does not depend on the translating speed. This cannot be clearly explained in this study, so a further investigation may be required

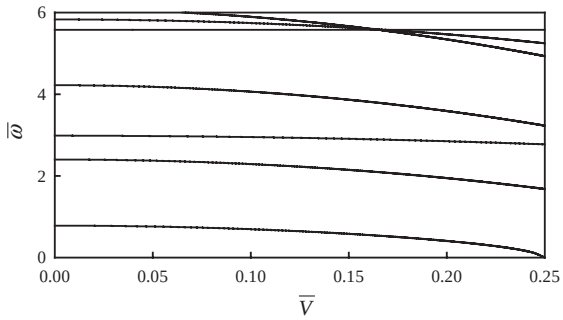

Fig. 7. Dimensionless natural frequencies $\bar{\omega}$ versus the dimensionless translating speed $\bar{V}$ for the membrane of Case II when $L/b = 3$.

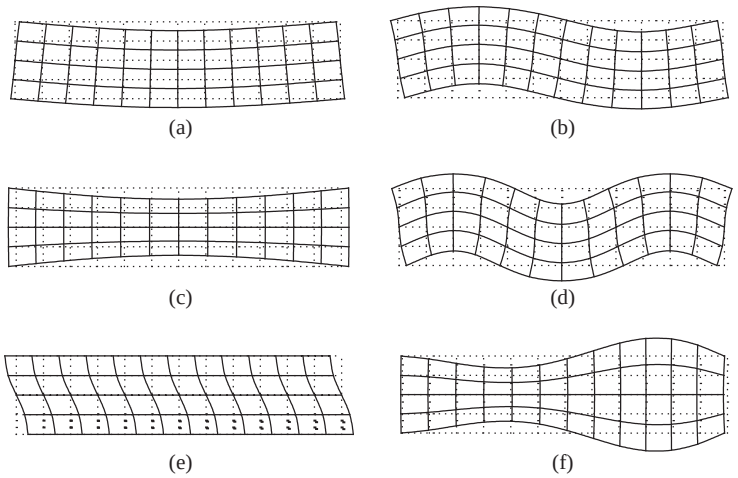

Fig. 8. Mode shapes of the membrane (Case II) when $L/b = 3$ and $\bar{V} = 0.01$: (a) the first mode; (b) the second mode; (c) the third mode; (d) the fourth mode; (e) the fifth mode; and (f) the sixth mode.

for why the natural frequency of the shear mode is independent of the translating speed. Recall that the shear mode is not found in Case I. On the other hand, the veering phenomena between the frequency loci are observed in Fig. 7, and the veering region is enlarged as shown in Fig. 9. In the region, it is seen that the corresponding modes are exchanged mutually.

Next, the effects of the aspect ratio on the lowest dimensionless natural frequency and the lowest critical speed are evaluated. As shown in Fig. 10, the natural frequencies diminish as not only the translating speed $\bar{V}$ but also the aspect ratio L/b increases. This trend is similar to that of Case I described in Fig. 5. A point to be noted from Figs. 5 and 10 is that the natural frequencies of Case II are much lower than those of Case I. This difference in magnitude is mainly due to boundary conditions. However, it seems that the critical speeds of Cases I and II are not much different. To investigate this relation between the critical speeds and boundary conditions, one more plot is generated as shown in Fig. 11. The vertical and horizontal axes denote the

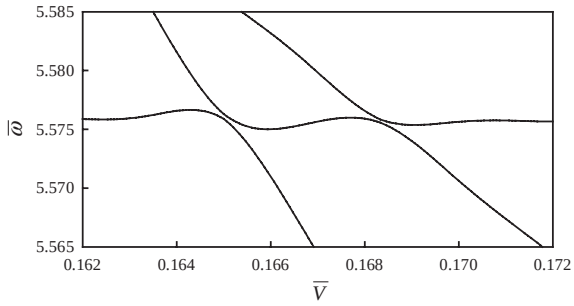

Fig. 9. Veering phenomena of the frequency loci (Case II).

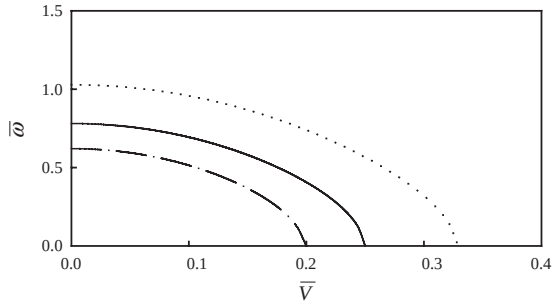

Fig. 10. Comparison of the lowest dimensionless natural frequency of the moving membrane for Case II when the aspect ratios are $L/b = 2$ (· · ·), 3 (—) and 4 (- · - · - · - ·).

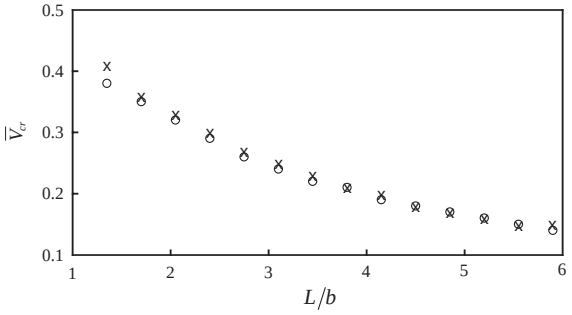

Fig. 11. Dimensionless critical speed $\bar{V}_{cr}$ versus aspect ratio L/b for Case I (o) and Case II (x).

dimensionless critical speed $\bar{V}_{cr}$ and aspect ratio L/b, respectively. It is seen that the critical speeds of both Cases I and II are almost the same for various aspect ratios. It is also seen that the critical speeds for both boundary conditions decrease as the aspect ratio increases. Thus, it can be stated that it is not the boundary conditions but the aspect ratio, which is a dominant player in determining the critical speed of moving membranes.

Fig. 12 shows the lowest four dimensionless natural frequencies as functions of the aspect ratio, where the solid and dotted lines denote $\bar{V} = 0.1$ and 0, respectively. These frequencies represent the

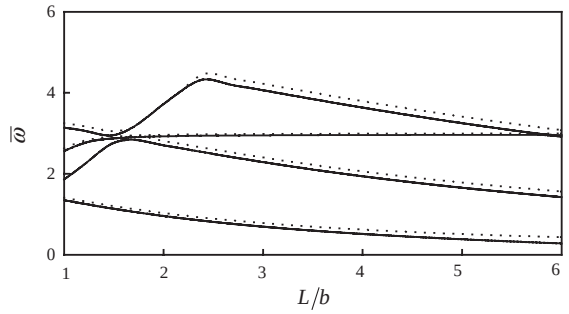

Fig. 12. Dimensionless natural frequencies $\bar{\omega}$ versus the aspect ratio L/b of the membrane of Case II when $\bar{V} = 0.1$ (—) or $\bar{V} = 0$ (· · ·).

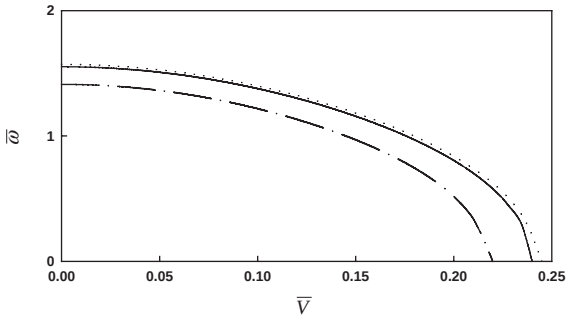

Fig. 13. The lowest dimensionless natural frequencies $\bar{\omega}$ versus the dimensionless translating speed $\bar{V}$ for the membranes (Case I, $L/b = 3$) of three different materials: magnetic tape (· · ·), aluminium (—) and soft rubber (- · - · - ·).

flexural and longitudinal modes. For example, the third lowest frequency at $L/b = 3$ is related to the longitudinal mode, and the others are frequencies of the flexural modes. It is seen that the frequencies of the moving membranes are lower than those of the stationary, but the trend of frequency loci is very similar to each other. It is also seen that, when the aspect ratio is higher than about 3, all the flexural frequencies decrease gradually with L/b. However, the longitudinal frequency grows slightly as the aspect ratio increases.

It can be noted from Figs. 6 and 12 that the longitudinal natural frequencies of Case II are almost the same as those of Case I for various aspect ratios. However, it is also observed in general that the flexural natural frequencies of Case II are much lower than those of Case I. Thus, the boundary conditions need to be properly considered in the in-plane vibration analysis of moving membranes because they have significant effects on the natural frequencies. It is, however, problematic to exactly define the boundary conditions of membranes on transport systems, and needs more investigations. For the lateral constraints between a membrane and rollers, it is recommended in further studies to adopt a friction model that may lie between Cases I and II of this study.

Finally, a result for the membranes of different materials is briefly presented. The dimensionless translating speed versus the lowest dimensionless natural frequencies of the membranes (Case I

and $L/b = 3$) made of three different materials: magnetic tape, aluminium ($\rho = 2700\,\mathrm{kg/m^3}$, $E = 71\,\mathrm{GPa}$ and $v = 0.33$) and soft rubber ($\rho = 950\,\mathrm{kg/m^3}$, $E = 5\,\mathrm{MPa}$ and $v = 0.5$) is shown in Fig. 13. It is found that even though the values of the dimensionless critical speed are slightly different, the trend is almost the same, and comments addressed for the membrane made of magnetic tape material are still applicable to those of different materials.

5. Summary and concluding remarks

The in-plane model of an axially moving membrane is developed, considering the effects of aspect ratio and translating speed. The equations of in-plane motion are derived by the extended Hamilton principle. At the boundaries with mass transport, two sets of boundary conditions (i.e., free and fixed constraints in the lateral direction) are considered. From the equations of motion and the associated boundary conditions, the weak form is obtained. The weak form is then discretized by using the Galerkin method. Based upon the discretized equations, the natural frequencies and mode shapes are computed. Especially, the effect of translating speed and aspect ratio on the in-plane vibration are investigated.

The results of this study can be summarized as follows.

(1) The natural frequencies of the flexural and longitudinal modes decrease as the translating speed increases.
(2) The natural frequency of the shear mode is independent of translating speed.
(3) The veering phenomena between frequency loci exist among the in-plane modes.
(4) The natural frequencies of the flexural modes decrease as the aspect ratio of moving membranes increases.
(5) The critical speed of the lowest frequency decreases as the aspect ratio increases.
(6) The critical speeds are almost the same for the two sets of boundary conditions.

Acknowledgements

This work was supported by the research fund of Hanyang University (Project No. HYU-2001-41).

References

[1] N.S. Bardell, R.S. Langiley, J.M. Dunsdon, On the free in-plane vibration of isotropic rectangular plates, *Journal of Sound and Vibration* 191 (1996) 459–467.
[2] K. Hyde, J.Y. Chang, C. Bacca, J.A. Wickert, Parameter studies for plane stress in-plane vibration of rectangular plates, *Journal of Sound and Vibration* 247 (2001) 471–487.
[3] Y. Kobayashi, G. Yamada, S. Honma, In-plane vibration of point-supported rectangular plates, *Journal of Sound and Vibration* 126 (1988) 545–549.
[4] A.N. Bercin, An assessment of the effects of in-plane vibrations on the energy flow between coupled plates, *Journal of Sound and Vibration* 191 (1996) 661–680.
[5] K.M. Liew, K.C. Hung, M.K. Lim, Three-dimensional vibration of rectangular plates: effects of thickness and edge constraints, *Journal of Sound and Vibration* 182 (1995) 709–727.

[6] J. Chung, C.S. Han, K. Yi, Vibration of an axially moving string with geometric non-linearity and translating acceleration, *Journal of Sound and Vibration* 240 (2001) 733–746.
[7] D.B. McIver, Hamilton's principle for systems of changing mass, *Journal of Engineering Mathematics* 7 (1972) 249–261.
[8] R. Sundaram, R.C. Benson, Tape dynamics following an impact, *IEEE Transactions on Magnetics* 26 (1990) 2211–2213.
[9] J. Chung, H.H. Yoo, Dynamic analysis of a rotating cantilever beam by using the finite element method, *Journal of Sound and Vibration* 249 (2002) 147–164.